

# Ultrathin Porous NiFeV Ternary Layer Hydroxide Nanosheets as a Highly Efficient Bifunctional Electrocatalyst for Overall Water Splitting

Dinh, Khang Ngoc; Zheng, Penglun; Dai, Zhengfei; Zhang, Yu; Dangol, Raksha; Zheng, Yun; Li, Bing; Zong, Yun; Yan, Qingyu

2017

Dinh, K. N., Zheng, P., Dai, Z., Zhang, Y., Dangol, R., Zheng, Y., et al. (2018). Ultrathin Porous NiFeV Ternary Layer Hydroxide Nanosheets as a Highly Efficient Bifunctional Electrocatalyst for Overall Water Splitting. *Small*, 14(8), 1703257-.

<https://hdl.handle.net/10356/88163>

<https://doi.org/10.1002/sml.201703257>

---

© 2017 WILEY-VCH Verlag GmbH & Co. KGaA, Weinheim. This is the author created version of a work that has been peer reviewed and accepted for publication by *Small*, WILEY-VCH Verlag GmbH & Co. KGaA, Weinheim. It incorporates referee's comments but changes resulting from the publishing process, such as copyediting, structural formatting, may not be reflected in this document. The published version is available at: [<http://dx.doi.org/10.1002/sml.201703257>].

*Downloaded on 27 Aug 2022 03:20:55 SGT*

DOI: 10.1002/ ((please add manuscript number))

Article type: Full Paper

## Ultrathin Porous NiFeV Ternary Layer Hydroxide Nanosheets as a Highly Efficient Bifunctional Electrocatalyst for Overall Water Splitting

*Khang Ngoc Dinh, Penglun Zheng, Zhengfei Dai,\* Yu Zhang, Raksha Dangol, Yun Zheng, Bing Li, Yun Zong, and Qingyu Yan\**

K. N. Dinh, Dr. Z. Dai Prof. Q. Yan

Energy Research Institute @ NTU (ERI@N), Interdisciplinary Graduate School, Nanyang Technological University, Singapore 637553, Singapore

E-mail: zfdai@ntu.edu.sg; alexyan@ntu.edu.sg

K. N. Dinh, P. Zheng, Dr. Z. Dai, Dr. Y. Zhang, D. Raksha, Dr. Y. Zheng, Prof. Q. Y. Yan

School of Materials Science and Engineering Nanyang Technological University, Singapore 639798, Singapore

E-mail: zfdai@ntu.edu.sg; alexyan@ntu.edu.sg

Dr. B. Li, and Dr. Y. Zong

Institute of Materials Research and Engineering, A\*STAR (Agency for Science, Technology and Research), 2 Fusionopolis Way Innovis #08-03, Singapore 138634, Singapore

Keywords: Overall water splitting; two-dimensional materials; layer double hydroxides; electrocatalysis; porous nanosheets

**Abstract.** Herein, we report the hydrothermal synthesis of porous ultrathin ternary NiFeV layer double hydroxides (LDHs) nanosheets grown on Nickel foam (NF) substrate as a highly efficient electrode toward overall water splitting in alkaline media. The lateral size of the nanosheets is about few hundreds of nanometers with the thickness of ~10 nanometers. Among all molar ratio investigated, the Ni<sub>0.75</sub>Fe<sub>0.125</sub>V<sub>0.125</sub>-LDHs/NF electrode depicts the optimized performance. It displays an excellent catalytic activity with a modest overpotential of 231 mV for oxygen evolution reaction (OER) and 125 mV for hydrogen evolution reaction (HER) in 1.0 M KOH electrolyte. Its exceptional activity is further shown in its small Tafel slope of 39.4 mV dec<sup>-1</sup> and 62.0 mV dec<sup>-1</sup> for OER and HER, respectively. More importantly, remarkable durability and stability are also observed. When used for overall water splitting, the Ni<sub>0.75</sub>Fe<sub>0.125</sub>V<sub>0.125</sub>-

1  
2  
3  
4 **LDHs**/NF electrodes require a voltage of only 1.591 V to reach 10 mA cm<sup>-2</sup> in alkaline solution.  
5

6  
7 These outstanding performances are mainly attributed to the synergistic effect of the ternary  
8  
9 metal system that boosts the intrinsic catalytic activity and active surface area. This work  
10  
11 explores a promising way to achieve the optimal inexpensive Ni-based hydroxide electrocatalyst  
12  
13  
14 for overall water splitting.  
15  
16  
17  
18  
19  
20  
21  
22  
23  
24  
25  
26  
27  
28  
29  
30  
31  
32  
33  
34  
35  
36  
37  
38  
39  
40  
41  
42  
43  
44  
45  
46  
47  
48  
49  
50  
51  
52  
53  
54  
55  
56  
57  
58  
59  
60  
61  
62  
63  
64  
65

## 1. Introduction

Hydrogen is considered as an environmentally friendly fuel, which can be produced by water electrolysis.<sup>[1]</sup> However, one of the key issue in electrocatalytic water splitting is the kinetic losses while driving oxygen evolution reaction (OER) at the anode and hydrogen evolution reaction (HER) at the cathode.<sup>[2,3]</sup> Besides, excess bubbling at the electrode surface is another limitation hindering the electrochemical water splitting. The catalyst may possibly peel off from the current collector under high current densities due to the oxygen and hydrogen bubbling.<sup>[4,5]</sup> These problems result in the decrease in catalytic activity of the catalyst. By now, the state-of-the-art HER and OER electrocatalysts are based on precious metals which are reported to display the lowest overpotentials at practical current densities. For example, RuO<sub>2</sub> exhibit an onset overpotential of about 140 mV to drive OER in alkaline solution while Pt displays nearly zero onset potential for HER under acidic condition.<sup>[1,6-8]</sup> Nevertheless, because of their high cost and scarcity, the practical applications of these materials in water electrolysis is limited.<sup>[9]</sup> Also, in order to realize overall water splitting, the coupling of HER and OER electrocatalysts in the same electrolyte is a great challenge since the most of the current approaches show the contradictory integration of HER and OER electrocatalysts; thus, leading to low efficiency. Hence, the discovery of earth-abundant, low-cost, high activity bifunctional electrocatalysts to achieve low energy-intensive water electrolysis is still highly desired. A wide range of earth abundant catalytic materials with different morphologies, structure or loaded on various substrates have been developed for OER and HER, including transition metal oxides/hydroxides,<sup>[10-15]</sup> carbides,<sup>[16-18]</sup> and phosphides.<sup>[19-21]</sup> Nevertheless, as stated in recent report, metal chalcogenides, nitrides, and phosphides are very sensitive in the strongly oxidizing OER conditions.<sup>[22]</sup> Thus, researches should not refer to these unstable material as OER

1  
2  
3  
4 electrocatalyst or bifunctional HER/OER catalyst in general. Recent years, nickel based layered  
5  
6 hydroxides with exceptional HER, OER activity and stability are demonstrated as the promising  
7  
8 alternatives to the conventional precious metal-containing water splitting catalysts in basic  
9  
10 solutions.<sup>[23-25]</sup> A representative compound in that family, NiFe layer double hydroxides (LDHs),  
11  
12 has been reported to be one of the best performing bifunctional electrocatalyst so far, in which  
13  
14 the integration of Fe is essential for high catalytic activity.<sup>[24,26]</sup> However, the limited specific  
15  
16 surface area and poor electronic conductivity of the Ni based hydroxides hinders its practical  
17  
18 application as an electrode material.  
19  
20  
21  
22

23  
24 To overcome this issue, elemental doping could be an effective approach to tune the  
25  
26 catalytic activity of the electrocatalyst. For instance, NiV-LDHs was reported to show enhanced  
27  
28 intrinsic catalytic property toward OER due to better conductivity and richer active sites; the  
29  
30 theoretical calculation also indicated that vanadium doping could significantly lower the  
31  
32 overpotential for the rate-determining step.<sup>[27]</sup> Another work recently highlights that the  
33  
34 Aluminum doping is found to be very advantageous since it would help to increase the number  
35  
36 of active sites when Al atoms are partially etched under strong alkaline media.<sup>[28]</sup> Also, to the  
37  
38 extent of our knowledge, not many studies have reported HER and overall water electrolysis  
39  
40 catalytic activity of layer hydroxide material in alkaline condition. Inspired by these analyses, it  
41  
42 is reasonable to expect that **triple metal** Ni-based **LDHs** may synergistically combine the  
43  
44 advantages of each component and show superior water splitting catalytic activity, which has not  
45  
46 been well explored.  
47  
48  
49  
50  
51  
52

53 In this study, we reported the preparation of NiFeV-**LDHs** nanosheets grown on nickel foam  
54  
55 (NiFeV-**LDHs**/NF). The nanosheets are porous with the lateral size of few hundreds of  
56  
57 nanometers and the thickness of ~10 nanometers. These porous nanosheets stack together to  
58  
59  
60  
61  
62  
63  
64  
65

form a flower-like structure. As a result, sufficient space for electrolyte penetration and diffusion is provided, which helps to expose more active sites. When used as an electrocatalytic electrode for OER and HER in alkaline solution (pH=14), the Ni<sub>0.75</sub>Fe<sub>0.125</sub>V<sub>0.125</sub>-LDHs/NF shows the optimized catalytic activity among all compositions investigated. It depicted extremely low operating overpotential (231 mV at 10 mA cm<sup>-2</sup>) combined with a modest Tafel slope (39.4 mV dec<sup>-1</sup>) for OER. An exceptional HER activity is also acquired with an overpotential of only 125 mV at 10 mA cm<sup>-2</sup> and a small Tafel slope of 62.0 mV dec<sup>-1</sup>. As an integrated electrocatalyst for water electrolysis, the cell exhibits a voltage of merely 1.591 V at 10 mA cm<sup>-2</sup>. In addition, the catalyst displays superb long-term stability when continuously operating at 30 mA cm<sup>-2</sup> for 15 hours. This work opens up a new route to further optimizing the Ni-based hydroxides materials for better electrochemical overall water splitting to replace precious transition metal catalysts.

## 2. Results and Discussion

### 2.1. Characterization of NiFeV-LDHs nanosheets.

A simplified hydrothermal treatment was utilized to synthesize the NiFeV-LDHs/NF employing Nickel chloride, iron (III) chloride, and Vanadium (III) chloride (with a molar ratio of Ni/Fe/V = 6/1/1) as metal precursors and urea as precipitant at 120 °C for 16 h (see Experimental section for details).

Without addition of Fe and V, the diffraction peaks at 11.4, 22.7, 34.0, 38.8, 46.0, 60.1, 61.3° in **Figure 1a** (blue) confirm the formation of hexagonal  $\alpha$ -Ni(OH)<sub>2</sub> · 0.75H<sub>2</sub>O (JCPDS card No. 038-0715, a=3.080, c=23.410; the peaks mark “\*” at 44.5, 51.9, 76.4° belong to the Ni foam substrate). The XRD pattern of the sample with the presence of Fe and V (in red) unveils that NiFeV-LDHs and  $\alpha$ -Ni(OH)<sub>2</sub> · 0.75H<sub>2</sub>O are isomorphous, which is consistent with previous reports on Ni-based hydroxides materials.<sup>[26,27]</sup> X-ray photoelectron spectroscopy (XPS) were

also conducted to confirm the presence of Ni, Fe, V in the catalyst and study their oxidation states in the materials (**Figure 1b-d and Figure S1**, Supporting Information). As shown in the Ni 2p spectrum (Figure 1b), the main peaks of Ni 2p<sub>3/2</sub> and 2p<sub>1/2</sub> are clearly observed at 854.6 eV and 872.1 eV, respectively; along with a satellite peak at 860.0 eV. The spin energy separation is roughly 17.5 eV indicating the presence of the Ni<sup>2+</sup> as reported in the literature.<sup>[29,30]</sup> The Fe 2p XPS spectrum (Figure 1c) reveals two peaks at binding energy of 710.9 eV and 724.1 eV, which correspond to Fe 2p<sub>3/2</sub> and 2p<sub>1/2</sub> and are the characteristic peaks of Fe<sup>3+</sup>.<sup>[31-33]</sup> In the V 2p spectrum (Figure 1d), there is a pair of peak separated by approximately 7.6 eV at 515.0 eV and 522.6 eV, which is ascribed to V 2p<sub>3/2</sub> and V 2p<sub>1/2</sub> due to p orbital j-j coupling (as the peak area ratio is 2:1). The deconvolution of V 2p<sub>3/2</sub> region in V 2p spectrum indicates three well-resolved contributions at ~513.9 eV (in red), ~515.0 eV (in blue) and ~515.9 eV (in purple), which belong to V<sup>3+</sup>, V<sup>4+</sup>, and V<sup>5+</sup>, respectively.<sup>[34-36]</sup> This result is also consistent with the finding of earlier study that indicated the partial oxidation of V<sup>3+</sup> to V<sup>4+</sup> and V<sup>5+</sup> during the LDHs synthesis.<sup>[27]</sup> Scanning electron microscopy (SEM) images of the as-prepared NiFeV-LDHs/NF is illustrated in **Figure 2a**, which shows that the NiFeV double hydroxide nanosheets were uniformly grown on the surfaces of NF substrate. In addition, the nanosheets stack together to form a porous flower-like structure. This kind of porous structure may be beneficial for electrolyte penetration and diffusion. For transmission electron microscopy (TEM) analysis, the as-prepared NiFeV-LDHs/NF was vigorously sonicated in ethanol to disperse the NiFeV-LDHs nanosheets into solution, which was then dropped onto TEM grids. The TEM images of NiFeV-LDHs nanosheets are shown in Figure 2b-c, which are almost transparent due to ultrathin nature. A closer look on the nanosheets (Figure 2g) clearly indicates the nanoporous structure of the material, which is beneficial to expose more active sites. The TEM image of vertically aligned

NiFeV-LDHs nanosheets shows the thickness of ~10 nm (Figure S2, Supporting Information). High resolution TEM (HRTEM) image taken from the nanosheet (Figure 2d) displays well-resolved lattice fringes with an interplanar spacing of 0.232 nm and 0.260 nm indexed to the (015) and (012) plane; respectively, of the hexagonal phase (JCPDS card No. 038-0715). The selected area electron diffraction (SAED) pattern (Figure 2e) exhibits the 6-fold point pattern. This result further confirms the hexagonal phase of the NiFeV-LDHs as we see earlier in the diffractogram. The High-Angle Annular Dark Field (HAADF) images and Scanning Transmission Electron Microscopes-Energy Dispersive X-ray spectroscopy (STEM-EDX) elemental mapping images shows that nickel, iron, and vanadium are uniformly distributed and overlapped all over the nanosheets (Figure 2g-j).

## 2.2. OER performances of NiFeV-LDHs/NF electrodes.

To gain insight into the electrochemical activities of NiFeV-LDHs, we firstly examined the NiFeV-LDHs/NF for OER in O<sub>2</sub> saturated 1.0 M KOH solution at a slow scan rate of 1 mV s<sup>-1</sup> to minimize the capacitive current using a typical three-electrode setup using Pt plate and the calibrated Hg/HgO (Figure S3, Supporting Information) as the counter electrode and reference electrode, respectively. All the electrocatalytic measurements were performed at room temperature and potentials reported in this work are *versus* Reversible Hydrogen Electrode (RHE). For comparison purposes, the OER activities of NiFe-LDHs/NF (Ni:Fe = 3:1, molar ratio), NiV-LDHs/NF (Ni:V = 3:1), Ni(OH)<sub>2</sub>/NF and bare Ni foam were investigated. We also examined the OER activities of NiFeV-LDHs/NF electrodes with different elemental ratio to optimize the composition. The elemental ratio of Ni, Fe, and V in all synthesized LDHs has been quantified by ICP-OES (Table S1, Supporting Information), revealing the atomic ratios of Ni: Fe: V are close to what were used in the corresponding syntheses. It is shown that the



Ni<sub>0.75</sub>Fe<sub>0.125</sub>V<sub>0.125</sub>-LDHs/NF electrode displays an optimal OER catalytic activity an overpotential of 231 mV at 10 mA cm<sup>-2</sup> and Tafel slope of 39.4 mV dec<sup>-1</sup> (Figure S4a-b, Supporting Information).

Figure 3a displays the polarization curves with IR compensation. It is notable that the bare Ni foam gives insignificant OER activity in the tested potential range (Figure S5, Supporting Information). In contrast, the Ni<sub>0.75</sub>Fe<sub>0.125</sub>V<sub>0.125</sub>-LDHs/NF electrodes exhibit an onset overpotential of 228 mV, which is much lower than those of NiFe-LDHs/NF (274 mV), NiV-LDHs/NF (252 mV), and Ni(OH)<sub>2</sub>/NF (340 mV). In addition, it can be seen that the anodic current density rises abruptly at higher positive potentials. The superior activity of the Ni<sub>0.75</sub>Fe<sub>0.125</sub>V<sub>0.125</sub>-LDHs/NF electrode is further shown in its small Tafel slope of 39.4 mV dec<sup>-1</sup> (Figure 3b), which is lower than those of NiFe-LDHs/NF (65.7 mV dec<sup>-1</sup>), NiV-LDHs/NF (54.1 mV dec<sup>-1</sup>), and Ni(OH)<sub>2</sub>/NF (95.9 mV dec<sup>-1</sup>). It is worth noting that the flat Tafel slope of Ni<sub>0.75</sub>Fe<sub>0.125</sub>V<sub>0.125</sub>-LDHs/NF electrode is in the range of 30-40 mV dec<sup>-1</sup>, which indicates the rate-determining characteristic for the second step (\*OH → \*O + H<sup>+</sup> + e<sup>-</sup>).<sup>[37]</sup> Practically, the overpotential to drive a current density of 10 mA cm<sup>-2</sup> is another important parameter since solar-light-coupled water splitting system normally run at 10 mA cm<sup>-2</sup> under standard conditions (1 sun, AM 1.5).<sup>[1]</sup> At 10 mA cm<sup>-2</sup>, the optimized layer double hydroxides of Ni<sub>0.75</sub>Fe<sub>0.125</sub>V<sub>0.125</sub>-LDHs/NF shows a low overpotential of only 231 mV, which is much less than NiFe-LDHs/NF (278 mV), NiV-LDHs/NF (257 mV), and Ni(OH)<sub>2</sub>/NF (347 mV) (Figure 3c). To the best of our knowledge, this overpotential is lower than the most of reported layer hydroxide materials (Table S2, Supporting Information). The long-term stability of the as-prepared Ni<sub>0.75</sub>Fe<sub>0.125</sub>V<sub>0.125</sub>-LDHs/NF electrode was also examined in 1.0 M KOH solution by chronopotentiometry method at fixed current density of 30 mA cm<sup>-2</sup> (Figure 3d). It can be seen

1  
2  
3  
4 that a stable operating potential is obtained for 15 hours of polarization (well below 1% change),  
5  
6 suggesting the remarkable durability of the electrode. The crystallinity and morphology are well  
7  
8 preserved after 15 hours of stability test, indicating the structural robustness of the electrode  
9  
10 (Figure 3d, inset and **Figure S6a-b**, Supporting Information). In addition, to prove that all the  
11  
12 current is due to water oxidation, the theoretical and experimental O<sub>2</sub> evolved by  
13  
14 Ni<sub>0.75</sub>Fe<sub>0.125</sub>V<sub>0.125</sub>-LDHs/NF electrode at a constant current of 10 mA were carried out (**Figure**  
15  
16 **S7**, Supporting Information). The experimental O<sub>2</sub> was measured by gas chromatography,  
17  
18 showing ~100% Faradaic efficiency for 60 minutes of electrolysis.  
19  
20  
21  
22

### 23 2.3. HER performances of NiFeV-LDHs/NF electrodes.

24  
25 We also probed HER electrocatalytic activity of NiFeV-LDHs catalyst in 1.0 M KOH electrolyte  
26  
27 using a typical three-electrode setup using Graphite rod as the counter electrode and the  
28  
29 calibrated Hg/HgO as the reference electrode. To explore the optimized composition of NiFeV-  
30  
31 LDHs for HER, LSV measurements at 1 mV s<sup>-1</sup> of samples with different metal ratio were conducted  
32  
33 (**Figure S8a-b**, Supporting Information), once again confirming the best HER catalytic activity of  
34  
35 Ni<sub>0.75</sub>Fe<sub>0.125</sub>V<sub>0.125</sub>-LDHs/NF electrode, which shows an overpotential of 125 mV at 10 mV cm<sup>-2</sup>  
36  
37 and a small Tafel slope of 62.0 mV dec<sup>-1</sup>.  
38  
39  
40  
41  
42

43 **Figure 4a** illustrates the LSV curves of NiFeV-LDHs/NF, NiV-LDHs/NF, NiFe-LDHs/NF, and  
44  
45 Ni(OH)<sub>2</sub>/NF catalytic electrodes at a scan rate of 1 mV s<sup>-1</sup>. Firstly, it should be noted that Ni foam  
46  
47 gives a minor current density in the tested potential range (**Figure S9**, Supporting Information).  
48  
49 Compared to other control catalysts, the Ni<sub>0.75</sub>Fe<sub>0.125</sub>V<sub>0.125</sub>-LDHs/NF electrode shows noticeably  
50  
51 improved HER performance with an onset overpotential of 86 mV and a modest Tafel slope of 62.0  
52  
53 mV dec<sup>-1</sup> (Figure 4b) indicating that the HER proceeds through Volmer- Heyrovsky mechanism, in  
54  
55 which the Volmer reaction (M<sub>cat</sub> + H<sub>2</sub>O + e<sup>-</sup> ⇌ M<sub>cat</sub>H<sub>ad</sub> + OH<sup>-</sup>) is the rate-determining step.<sup>[38]</sup>  
56  
57  
58  
59  
60  
61  
62  
63  
64  
65

Moreover, an overpotential to drive a current density of  $10 \text{ mA cm}^{-2}$  of 125 mV is achieved (Figure 4c), revealing a superior cathode for hydrogen generation in alkaline electrolyte (pH=14); meanwhile Ni(OH)<sub>2</sub>/NF, NiFe-LDHs/NF, NiV-LDHs/NF require 193 mV, 157 mV, 145 mV, respectively. The HER electrocatalysis durability is also crucial for practical application. Figure 4d reveals the chronopotentiometry test for the Ni<sub>0.75</sub>Fe<sub>0.125</sub>V<sub>0.125</sub>-LDHs/NF electrode performed in 1.0 M KOH at the current density of  $-30 \text{ mA cm}^{-2}$ . An insignificant voltage increase of just above 1% over 15 hours and the post analysis studies (Figure 4d; **Figure S10a-b**, Supporting Information) suggest that the Ni<sub>0.75</sub>Fe<sub>0.125</sub>V<sub>0.125</sub>-LDHs own an excellent stability and HER durability in strong alkaline solution (pH=14). Also, the Ni<sub>0.75</sub>Fe<sub>0.125</sub>V<sub>0.125</sub>-LDHs/NF electrode exhibits almost 100% Faradaic efficiency under constant current of  $-10 \text{ mA}$  for 60 minutes (**Figure S11**, Supporting Information)

#### 2.4. Characterizations and overall water splitting performances.

The above results and discussions indicate that the Ni<sub>0.75</sub>Fe<sub>0.125</sub>V<sub>0.125</sub>-LDHs is a highly active and stable electrocatalyst for both OER and HER in strong alkaline medium (pH=14). Hence, a homemade two-electrode set up with Ni<sub>0.75</sub>Fe<sub>0.125</sub>V<sub>0.125</sub>-LDHs/NF as both anode and cathode was employed to investigate the electrocatalytic activity toward water electrolysis in 1.0 M KOH solution. During water splitting, bubbles were clearly observed on surfaces of both electrodes (**Figure S12 and Supplementary video S1**, Supporting Information). The voltage to reach a current density of  $10 \text{ mA cm}^{-2}$  is found to be 1.591 V, surpassing the state-of-the-art IrO<sub>2</sub>/NF-Pt/C/NF which requires 1.738 mV (**Figure 5a**). In chronopotentiometry test, the cell remains stable overpotential (less than 2% increment) at  $30 \text{ mA cm}^{-2}$  after 15 hours of operation (Figure 5b). The overpotential at  $10 \text{ mA cm}^{-2}$  obtained using a two-electrode system (361 mV) is very similar to that of the three-electrode system (356 mV, combining HER and OER), between which the 5 mV difference is due to the different testing configurations.<sup>[39]</sup> A related point to consider is that the onset potential of the

Ni<sub>0.75</sub>Fe<sub>0.125</sub>V<sub>0.125</sub>-LDHs/NF based electrolyzer cell is 1.491 V; hence, a single battery unit of 1.5 V is able to drive the water splitting (**Figure S12**, Supporting Information). As is evident from **Supplementary video S2**, small gas bubbles are released from the surface of the electrodes, indicating the successful splitting of water with only 0.27 V overpotential. This performance of Ni<sub>0.75</sub>Fe<sub>0.125</sub>V<sub>0.125</sub>-LDHs/NF electrodes is remarkably impressive compared to that of reported bifunctional catalysts and even benchmark catalysts (**Table S4**, Supporting Information).

In light of the excellent electrochemical properties toward OER, HER, and overall water splitting of the Ni<sub>0.75</sub>Fe<sub>0.125</sub>V<sub>0.125</sub>-LDHs catalyst, it is necessary to estimate the electrochemically effective surface area (ECSA) since higher active surface area results in higher number of active sites and normally better catalytic activity. Cyclic voltammetry (CV) was conducted in a potential window of 0.3–0.4 V (vs. Hg/HgO reference electrode) at various scan rate of 2, 4, 6, 8, 10, and 12 mV s<sup>-1</sup> (**Figure S14a-g**, Supporting Information). Then by plotting capacitive current ( $j_{\text{anodic}} - j_{\text{cathodic}}$ ) at 0.35 V against scan rates, a obtained linear slope is equivalent to twice of the double layer capacitance ( $C_{\text{dl}}$ ) value, which is employed to represent the ECSA.<sup>[40]</sup> As shown in **Figure 6a**, the electrochemical results reveal that the Ni<sub>0.75</sub>Fe<sub>0.125</sub>V<sub>0.125</sub>-LDHs/NF has a  $C_{\text{dl}}$  of 126.2 mF cm<sup>-2</sup>, which is higher than NiFe-LDHs/NF (39.5 mF cm<sup>-2</sup>), NiV-LDHs/NF (96.3 mF cm<sup>-2</sup>), and Ni(OH)<sub>2</sub>/NF (41.4 mF cm<sup>-2</sup>). This implies that Ni<sub>0.75</sub>Fe<sub>0.125</sub>V<sub>0.125</sub>-LDHs/NF has a larger electroactive surface area, which partially facilitates the reactions. Nonetheless, it has not escaped our notice that compared to the best **double metal** LDHs in this study, Ni<sub>0.75</sub>Fe<sub>0.125</sub>V<sub>0.125</sub>-LDHs/NF has only 1.3-fold higher in ECSA; with such small increase of active sites, the current density at 280 mV **OER overpotential** is well above six times larger (178.5 mA cm<sup>-2</sup> compared to 28.2 mA cm<sup>-2</sup>). This analysis suggests that such significant enhancement cannot be only attributed to the marginally increased effective surface area but also higher intrinsic activity of

1  
2  
3  
4 the  $\text{Ni}_{0.75}\text{Fe}_{0.125}\text{V}_{0.125}$ -LDHs/NF electrode. The ECSAs of NiFeV-LDHs/NF with different  
5  
6 compositions were further examined in details. The  $C_{dl}$  of  $\text{Ni}_{0.5}\text{Fe}_{0.25}\text{V}_{0.25}$ -,  $\text{Ni}_{0.66}\text{Fe}_{0.167}\text{V}_{0.167}$ -,  
7  
8  $\text{Ni}_{0.75}\text{Fe}_{0.125}\text{V}_{0.125}$ - and  $\text{Ni}_{0.8}\text{Fe}_{0.1}\text{V}_{0.1}$ -LDHs/NF electrodes were 89.4, 82.8, 126.2, and 60.3 mF  
9  
10  $\text{cm}^{-2}$ , respectively (Figure S14h, Supporting Information). The  $\text{Ni}_{0.75}\text{Fe}_{0.125}\text{V}_{0.125}$ -LDHs/NF  
11  
12 electrode possesses the optimum ECSA, implying that the number of surface active sites can be  
13  
14 increased by optimizing the ratio of three metal in the system. It is also noted that although the  
15  
16 current density of NiFeV-LDHs/NF with different ratio show an increase trend along with ECSA,  
17  
18 only doubling the ECSA (from 60.3 to 126.2 mF  $\text{cm}^{-2}$ ) leads to more than 8 times current density  
19  
20 improvement (from ~21.5 to 178.5 mA  $\text{cm}^{-2}$ ) (Figure S15, Supporting Information). This is a  
21  
22 solid evidence that optimizing Ni, Fe, and V ratio not only boost the surface active sites, but also  
23  
24 increase the intrinsic activity.  
25  
26  
27  
28  
29  
30

31 To further investigate the kinetics of the as-obtained catalysts, electrochemical impedance  
32  
33 spectroscopy (EIS) measurements were carried out at a potential of 1.53 V (vs. RHE) in the  
34  
35 frequency range from 100 kHz to 0.1 Hz in 1.0 M KOH solution. Figure 6b shows the Nyquist  
36  
37 plots that were fitted by a reported electrical analog.<sup>[41]</sup> The x-intercepts at high frequency region  
38  
39 indicate the solution resistance, which were used for Ohmic correction in this study. The charge-  
40  
41 transfer resistance ( $R_{ct}$ ), corresponding to the semicircular diameter in the EIS spectrum, of  
42  
43  $\text{Ni}_{0.75}\text{Fe}_{0.125}\text{V}_{0.125}$ -LDHs/NF electrode is only 0.50  $\Omega$ , slightly smaller than those of other control  
44  
45 samples, e.g. 0.57  $\Omega$  ( $\text{Ni}(\text{OH})_2/\text{NF}$ ), 0.52  $\Omega$  (NiV-LDHs/NF), and 0.64  $\Omega$  (NiFe-LDHs/NF).  
46  
47 These small resistances are ascribed to the superb electrical contact between the catalyst and  
48  
49 conductive Ni foam support. In addition, the smaller  $R_{ct}$  of the optimized  $\text{Ni}_{0.75}\text{Fe}_{0.125}\text{V}_{0.125}$ -  
50  
51 LDHs/NF electrode indicates faster charge transfer ability compared to other control electrodes.  
52  
53  
54  
55  
56  
57  
58  
59  
60  
61  
62  
63  
64  
65

To the best of our knowledge, the  $\text{Ni}_{0.75}\text{Fe}_{0.125}\text{V}_{0.125}$ -LDHs/NF electrode exhibits an outstanding OER performance, which is better than most of reported LDHs including the state-of-the-art NiFe-LDHs. Also, to successfully drive the water splitting with a single 1.5 V battery, the phenomenal HER performance in 1.0 M KOH solution, which has not been well explored for hydroxide materials, should be taken into account (Table S2-S4, Supporting Information). The exceptional catalytic activity is attributed to the synergistically combination of Fe and V in Ni-based layer hydroxide that leads the better intrinsic catalytic activity and higher active surface area. The porous structure of the nanosheets gives enough space for electrolyte penetration and diffusion; as well as provide higher number of active sites by boosting the accessible ECSA. In addition, the in-situ growth of the hydroxide onto conductive Ni foam substrate benefits the charge transfer, lowering significantly the resistance of the system.

### 3. Conclusion

In summary, NiFeV-LDHs/NF with different molar ratio have been prepared by one-step hydrothermal treatment and demonstrated for the first time as highly active water splitting electrodes that outperform most of reported LDHs. Among all composition investigated,  $\text{Ni}_{0.75}\text{Fe}_{0.125}\text{V}_{0.125}$ -LDHs/NF delivers the best performance. To achieve a current density of 10  $\text{mA cm}^{-2}$ , it requires overpotentials of only 231 mV for OER and 125 mV for HER with a Tafel slope of 39.4  $\text{mV dec}^{-1}$  and 62.0  $\text{mV dec}^{-1}$ , respectively, in alkaline medium (pH=14). When integrated as both anode and cathode in water electrolysis, a modest voltage of 1.591 V is obtained to reach 10  $\text{mA cm}^{-2}$ . The electrode also exhibits outstanding durability and stability for 15 hours of operation at 30  $\text{mA cm}^{-2}$ . These excellent features come from the synergistic effect of ternary metals system and ultrathin porous nature of NiFeV-LDHs nanosheets. This work

opens up a new route to acquire the optimal low-cost Ni-based hydroxides materials for overall water splitting to eliminate the use of precious transition metal catalysts.

#### 4. Experimental Section

*Materials.* All the chemicals were purchased from Sigma-Aldrich and used without any further purification.

*Preparation of NiFeV-LDHs/NF, NiFe- and NiV-LDHs/NF, and Ni(OH)<sub>2</sub>/NF electrodes.*

The LDHs nanosheets grown on Ni foam were synthesized by hydrothermal method. In a typical synthesis, different mole ratios of Ni/Fe/V solution (2:1:1, 4:1:1, 6:1:1, 8:1:1, 3:1:0, 3:0:1, 1:0:0 for the synthesis of Ni<sub>0.5</sub>Fe<sub>0.25</sub>V<sub>0.25</sub>-LDHs/NF, Ni<sub>0.67</sub>Fe<sub>0.165</sub>V<sub>0.165</sub>-LDHs/NF, Ni<sub>0.75</sub>Fe<sub>0.125</sub>V<sub>0.125</sub>-LDHs/NF, Ni<sub>0.8</sub>Fe<sub>0.1</sub>V<sub>0.1</sub>-LDHs/NF, Ni<sub>0.75</sub>Fe<sub>0.25</sub>-LDHs/NF, Ni<sub>0.75</sub>V<sub>0.25</sub>-LDHs/NF, and Ni(OH)<sub>2</sub>/NF, respectively) were achieved by mixing NiCl<sub>2</sub>, FeCl<sub>3</sub> and VCl<sub>3</sub> in 20 ml H<sub>2</sub>O, while the total amount of metal cations (Ni<sup>2+</sup>, Fe<sup>3+</sup> and V<sup>3+</sup>) were kept at 1.2 mmol. Afterward, urea (500 mg) and NH<sub>4</sub>F (120 mg) were added, and the solution was stirred until a clear solution is formed. Nickel foam (2 cm × 0.5 cm) was cleaned with 6 M HCl solution in an ultrasonic bath for 10 minutes to clear away the surface oxide layer. After that, the Ni foam was rinsed with distilled water, acetone, and ethanol; followed by drying under Ar atmosphere. Then, the above mixture solution and the Ni foam were transferred to a 45-mL stainless-steel Teflon-lined autoclave and heated in an electric oven at 120 °C for 16 h. After cooling to room temperature, the as-synthesized hydroxides on Ni foam substrate was collected and subsequently rinsed with distilled water, ethanol, and dried in vacuum oven at 60 °C for 6 hours.

*Structure and surface characterization.* Thin film X-ray diffraction was performed to characterize the sample on the Shimadzu XRD-6000 X-ray diffractometer with Cu-K $\alpha$  irradiation ( $\lambda = 1.5406$  Angstrom). The morphology and structure of the materials were

1  
2  
3  
4 characterized using transmission electron microscopy with scanning transmission electron  
5  
6 microscopy (JEOL, Model JEM-2100F) operating at 200 keV, field emission scanning electron  
7  
8 microscopy (FESEM, JEOL, JSM-7600F) and atomic force microscopy (AFM) (Digital  
9  
10 Instruments). The energy-dispersive X-ray spectroscopy (EDX), elemental mapping and high  
11  
12 angle annular dark field scanning transmission electron microscopy (HAADF-STEM) were  
13  
14 performed by TEM (JEOL JEM 2100, 200 kV). The X-ray photoelectron spectroscopy (XPS,  
15  
16 VG Escalab 250 spectrometer) was conducted using Al anode with an energy source at 12 kV.

17  
18  
19  
20  
21 The Dual View Optima 5300 DV inductively coupled plasma-optical emission spectroscopy  
22  
23 (ICP-OES) was employed to analyze the composition of the synthesized LDHs

24  
25  
26 *Electrochemical measurements.* Electrochemical measurements were performed in a  
27  
28 conventional three-electrode system connected to Solartron electrochemical work station with  
29  
30 the as-prepared LDHs/NF as working electrodes, and Hg/HgO as the reference electrode. For  
31  
32 HER testing, graphite rod was employed as the counter electrode while platinum plate is used in  
33  
34 case of OER testing. All measurements were carried out in 1.0 M KOH electrolyte.  
35  
36  
37

38  
39 Prior to the test measurement, Hg/HgO electrode calibration was carried out in a three-  
40  
41 electrode system in which Pt wires served as both working electrode and counter electrode, and  
42  
43 Hg/HgO served as the reference electrode. H<sub>2</sub>-saturated 1.0 M KOH was employed as electrolyte.  
44  
45 Linear sweep voltammetry (LSV) was then conducted in the range of -0.8 to -1.0 V at a scan rate  
46  
47 of 0.5 mV s<sup>-1</sup> (H<sub>2</sub> was still purged during measurement). The potential at which the current  
48  
49 crosses zero was taken as thermodynamic potential (vs. Hg/HgO) for the hydrogen electrode  
50  
51 (Figure S3, Supporting Information). Thereby, all the potentials reported in our manuscript were  
52  
53 calibrated to a reversible hydrogen electrode (RHE) by using the equation:  $E_{\text{RHE}} = E_{\text{Hg/HgO}} +$   
54  
55  $0.917$ ; and overpotential  $\eta = E_{\text{RHE}} - 1.23\text{V}$ .  
56  
57  
58  
59  
60  
61  
62  
63  
64  
65



1  
2  
3  
4 LSV was then performed at scan rate of  $1 \text{ mV s}^{-1}$ . By plotting overpotential  $\eta$  vs. logarithm  
5  
6 of current density from polarization curves, Tafel slopes are obtained. To evaluate the durability  
7  
8 and stability of **LDHs** during HER and OER testing, a galvanostatic measurement at a fixed  
9  
10 current density of  $30 \text{ mA cm}^{-2}$  was conducted.

11  
12  
13  
14 The Faradaic efficiency of the  $\text{Ni}_{0.75}\text{Fe}_{0.125}\text{V}_{0.125}$ -LDHs/NF electrode was done in a Ar-  
15  
16 purged close H-shape cell (counter electrode was put in different chamber). The headspace of the  
17  
18 chamber containing working electrode is 20.0 mL. A constant current of -10 mA (or 10 mA in  
19  
20 case of OER) was applied for 60 minutes. The  $\text{H}_2$  (or  $\text{O}_2$ ) gas generated was determined by  
21  
22 taking 500  $\mu\text{l}$  of the gas sample in the chamber containing working electrode to gas  
23  
24 chromatography. The Faradaic efficiency was then calculated as the ratio of measured amount of  
25  
26  $\text{H}_2$  (or  $\text{O}_2$ ) and theoretical amount of  $\text{H}_2$  (or  $\text{O}_2$ ) (based on Faraday's law).  
27  
28  
29  
30

31 The electrochemical surface area (ESCA) was estimated from the double-layer capacitance  
32  
33 ( $C_{dl}$ ) of the films. The  $C_{dl}$  was determined by a simple cyclic voltammetry (CV) method. The CV  
34  
35 was conducted in a potential window (0.3-0.4 V vs. Hg/HgO) at various scan rates of 2, 4, 6, 8,  
36  
37 10, and  $12 \text{ mV s}^{-1}$ . Then capacitive current ( $j_{anodic} - j_{cathodic}$ ) at 0.35 V vs. Hg/HgO was plotted  
38  
39 against various scan rates, while the slope obtained was divided by two to acquire the  $C_{dl}$  value,  
40  
41 which represents ECSA.  
42  
43  
44

45 Overall water splitting tests were performed in a homemade two-electrode system with the  
46  
47  $\text{Ni}_{0.75}\text{Fe}_{0.125}\text{V}_{0.125}$ -**LDHs**/NF as both the cathode and anode. The mass loading was calculated to  
48  
49 be  $1.42 \text{ mg cm}^{-2}$ . For the benchmark noble metal-based catalysts,  $\text{IrO}_2$ /NF || Pt/C/NF was adopted  
50  
51 with the same mass loading as above sample. To specify, for the cathode, 10.143 mg of 10%  
52  
53 Pt/C was dispersed in 960  $\mu\text{l}$  isopropanol and 40  $\mu\text{l}$  5% Nafion; then, 35  $\mu\text{l}$  of the suspension was  
54  
55 coated on Ni foam (0.5 x 0.5 cm). The procedure to make the anode is similar except for the use  
56  
57  
58  
59  
60  
61  
62  
63  
64  
65

of IrO<sub>2</sub> instead of Pt/C. The LSV curves were performed in 1.0 M KOH at a scan rate of 1 mV s<sup>-1</sup> in the potential range of 1.0-2.0 V. The long-term durability was evaluated by constant current electrolysis.

The electrochemical impedance spectroscopy (EIS) measurements were performed with frequency from 0.1 Hz to 100 kHz at an amplitude of 10 mV. All results were corrected for all ohmic (IR) losses throughout the system based on the solution resistance obtained from the EIS.

### Supporting Information

Supporting Information is available from the Wiley Online Library or from the author.

### Acknowledgements

K. N. Dinh and P. L. Zheng contributed equally to this work. This work is financially supported by Singapore MOE AcRF Tier 1 grants 2016-T1-002-065, RG113/15, Singapore A\*STAR Pharos program SERC 1527200 022. We also would like to acknowledge the Facility for Analysis, Characterization, Testing and Simulation (FACTS), Nanyang Technological University, Singapore, for use of their electron microscopy and XRD facilities.

### Conflict of Interest

The authors declare no conflict of interest.

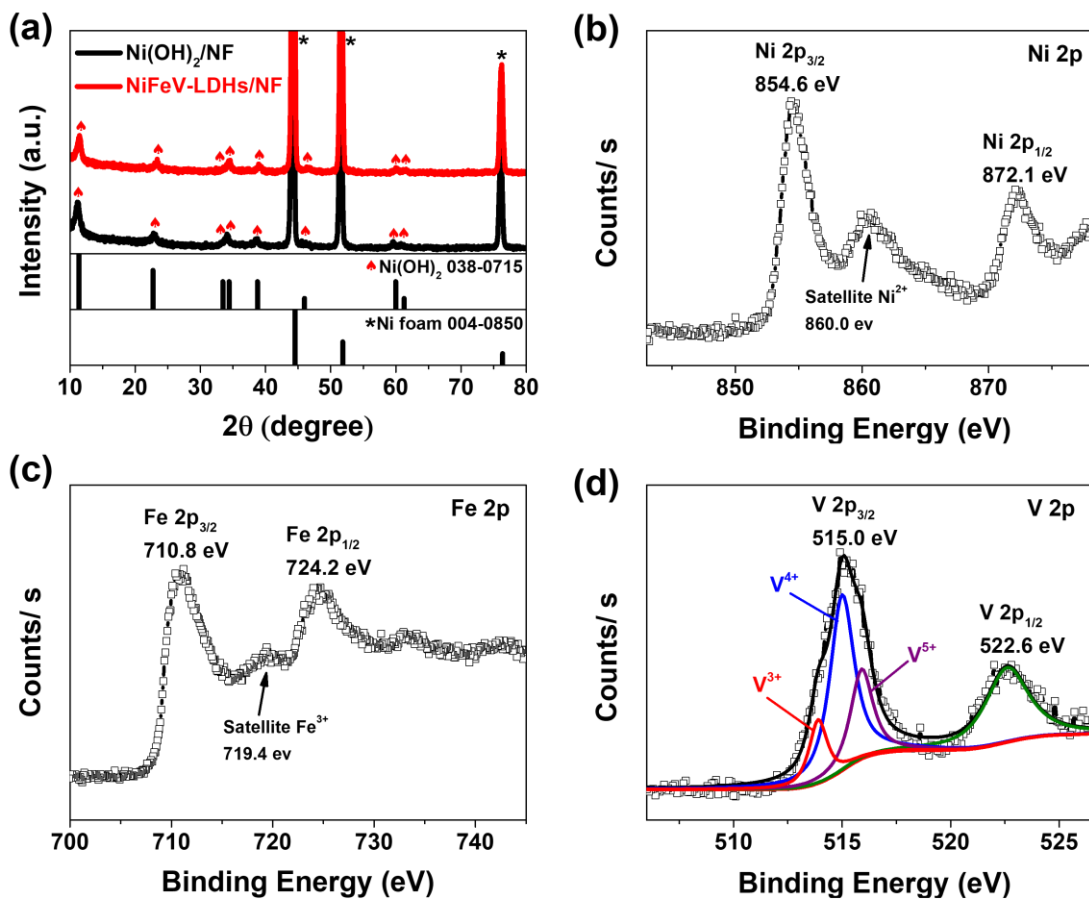
Received: ((will be filled in by the editorial staff))  
Revised: ((will be filled in by the editorial staff))  
Published online: ((will be filled in by the editorial staff))

## References

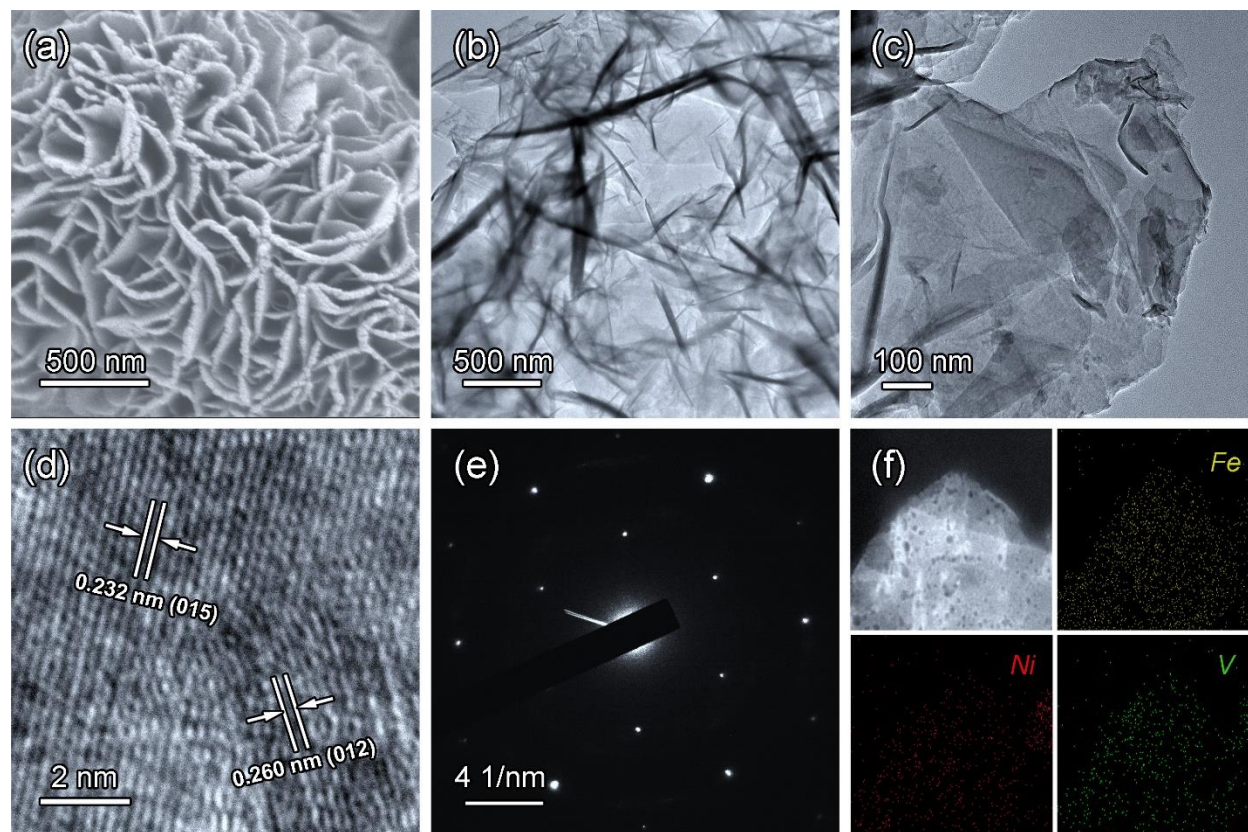
- [1] M. G. Walter, E. L. Warren, J. R. McKone, S. W. Boettcher, Q. Mi, E. A. Santori & N. S. Lewis, *Chem. Rev.* **2010**, 110, 6446.
- [2] F. Calle-Vallejo & M. T. M. Koper, *Electrochim. Acta* **2012**, 84, 3.
- [3] L. Ma, X. Luo, A. J. Kropf, J. Wen, X. Wang, S. Lee, D. J. Myers, D. Miller, T. Wu, J. Lu & K. Amine, *Nano Lett.* **2016**, 16, 781.
- [4] X. Lu & C. Zhao, *Nat. Commun.* **2015**, 6, 6616.
- [5] Z. Dai, U. Mani, H. T. Tan & Q. Yan, *Small Methods* **2017**, 1, 1700098.
- [6] N.-T. Suen, S.-F. Hung, Q. Quan, N. Zhang, Y.-J. Xu & H. M. Chen, *Chem. Soc. Rev.* **2017**, 46, 337.
- [7] J. Greeley, T. F. Jaramillo, J. Bonde, I. Chorkendorff & J. K. Norskov, *Nat. Mater.* **2006**, 5, 909.
- [8] D. Ansovini, C. J. Jun Lee, C. S. Chua, L. T. Ong, H. R. Tan, W. R. Webb, R. Raja & Y.-F. Lim, *J. Mater. Chem. A* **2016**, 4, 9744.
- [9] X. Liu, C. Meng & Y. Han, *J. Phys. Chem. C* **2013**, 117, 1350.
- [10] B. Weng, F. Xu, C. Wang, W. Meng, C. R. Grice & Y. Yan, *Energ. Environ. Sci.* **2017**, 10, 121.
- [11] Y. Zhao, C. Chang, F. Teng, Y. Zhao, G. Chen, R. Shi, G. I. N. Waterhouse, W. Huang & T. Zhang, *Adv. Energy Mater.*, DOI:10.1002/aenm.201700005.
- [12] R. Liu, Y. Wang, D. Liu, Y. Zou & S. Wang, *Adv. Mater.* **2017**, 29, 1701546.
- [13] Yiliguma, Z. Wang, W. Xu, Y. Wang, X. Cui, A. M. Al-Enizi, Y. Tang & G. Zheng, *J. Mater. Chem. A* **2017**, 5, 7416.
- [14] H. Wang, H.-W. Lee, Y. Deng, Z. Lu, P.-C. Hsu, Y. Liu, D. Lin & Y. Cui, *Nat. Commun.* **2015**, 6.
- [15] W. Liu, H. Liu, L. Dang, H. Zhang, X. Wu, B. Yang, Z. Li, X. Zhang, L. Lei & S. Jin, *Adv. Funct. Mater.* **2017**, 27, 1603904.
- [16] C. Lu, D. Tranca, J. Zhang, F. n. Rodríguez Hernández, Y. Su, X. Zhuang, F. Zhang, G. Seifert & X. Feng, *ACS Nano* **2017**, 11, 3933.
- [17] H. Fan, H. Yu, Y. Zhang, Y. Zheng, Y. Luo, Z. Dai, B. Li, Y. Zong & Q. Yan, *Angew. Chem. Int. Ed.*, DOI:10.1002/ange.201706610.
- [18] H. Wang, Y. Cao, C. Sun, G. Zou, J. Huang, X. Kuai, J. Zhao & L. Gao, *ChemSusChem*, DOI:10.1002/cssc.201701276.
- [19] J. Duan, S. Chen, A. Vasileff & S. Z. Qiao, *ACS Nano* **2016**, 10, 8738.
- [20] H. Duan, D. Li, Y. Tang, Y. He, S. Ji, R. Wang, H. Lv, P. P. Lopes, A. P. Paulikas, H. Li, S. X. Mao, C. Wang, N. M. Markovic, J. Li, V. R. Stamenkovic & Y. Li, *J. Am. Chem. Soc.* **2017**, 139, 5494.
- [21] X. Xiao, C.-T. He, S. Zhao, J. Li, W. Lin, Z. Yuan, Q. Zhang, S. Wang, L. Dai & D. Yu, *Energ. Environ. Sci.* **2017**, 10, 893.
- [22] S. Jin, *ACS Energy Lett.* **2017**, 2, 1937.
- [23] H. Liang, F. Meng, M. Cabán-Acevedo, L. Li, A. Forticaux, L. Xiu, Z. Wang & S. Jin, *Nano Lett.* **2015**, 15, 1421.
- [24] J. Luo, J.-H. Im, M. T. Mayer, M. Schreier, M. K. Nazeeruddin, N.-G. Park, S. D. Tilley, H. J. Fan & M. Grätzel, *Science* **2014**, 345, 1593.
- [25] H. Yin & Z. Tang, *Chem. Soc. Rev.* **2016**, 45, 4873.

- 1  
2  
3  
4 [26] M. Gong, Y. Li, H. Wang, Y. Liang, J. Z. Wu, J. Zhou, J. Wang, T. Regier, F. Wei & H.  
5 Dai, *J. Am. Chem. Soc.* **2013**, 135, 8452.  
6 [27] K. Fan, H. Chen, Y. Ji, H. Huang, P. M. Claesson, Q. Daniel, B. Philippe, H. Rensmo, F.  
7 Li, Y. Luo & L. Sun, *Nat. Commun.* **2016**, 7, 11981.  
8 [28] H. Liu, Y. Wang, X. Lu, Y. Hu, G. Zhu, R. Chen, L. Ma, H. Zhu, Z. Tie, J. Liu & Z. Jin,  
9 *Nano Energy* **2017**, 35, 350.  
10 [29] J. Yan, Z. Fan, W. Sun, G. Ning, T. Wei, Q. Zhang, R. Zhang, L. Zhi & F. Wei, *Adv.*  
11 *Funct. Mater.* **2012**, 22, 2632.  
12 [30] J. W. Lee, T. Ahn, D. Soundararajan, J. M. Ko & J.-D. Kim, *Chemi. Commun.* **2011**, 47,  
13 6305.  
14 [31] D. Wang, J. Zhou, Y. Hu, J. Yang, N. Han, Y. Li & T.-K. Sham, *J. Physical Chem. C*  
15 **2015**, 119, 19573.  
16 [32] W. Xiong, Q. Zhao, X. Li & L. Wang, *Part. Part. Syst. Char.* **2016**, 33, 602.  
17 [33] S. Xu, C. M. Hessel, H. Ren, R. Yu, Q. Jin, M. Yang, H. Zhao & D. Wang, *Energ.*  
18 *Environ. Sci.* **2014**, 7, 632.  
19 [34] M. C. Biesinger, L. W. M. Lau, A. R. Gerson & R. S. C. Smart, *Appl. Surf. Sci.* **2010**,  
20 257, 887.  
21 [35] H. Chen, Y. Deng, Z. Yu, H. Zhao, Q. Yao, X. Zou, J.-E. Bäckvall & J. Sun, *Chem.*  
22 *Mater.* **2013**, 25, 5031.  
23 [36] D. Lu, M. Zhang, Z. Zhang, Q. Li, X. Wang & J. Yang, *Nanoscale Res. Lett.* **2014**, 9,  
24 272.  
25 [37] E. B. Castro & C. A. Gervasi, *Int. J. Hydrogen Energ.* **2000**, 25, 1163.  
26 [38] C. Xu, S. Peng, C. Tan, H. Ang, H. Tan, H. Zhang & Q. Yan, *J. Mater. Chem. A* **2014**, 2,  
27 5597.  
28 [39] A. Sivantham, P. Ganesan & S. Shanmugam, *Adv. Funct. Mater.* **2016**, 26, 4661.  
29 [40] W. Ma, R. Ma, C. Wang, J. Liang, X. Liu, K. Zhou & T. Sasaki, *ACS Nano* **2015**, 9,  
30 1977.  
31 [41] J. Liu, J. Wang, B. Zhang, Y. Ruan, L. Lv, X. Ji, K. Xu, L. Miao & J. Jiang, *ACS Appl.*  
32 *Mater. Inter.* **2017**, 9, 15364.  
33  
34  
35  
36  
37  
38  
39  
40  
41  
42  
43  
44  
45  
46  
47  
48  
49  
50  
51  
52  
53  
54  
55  
56  
57  
58  
59  
60  
61  
62  
63  
64  
65

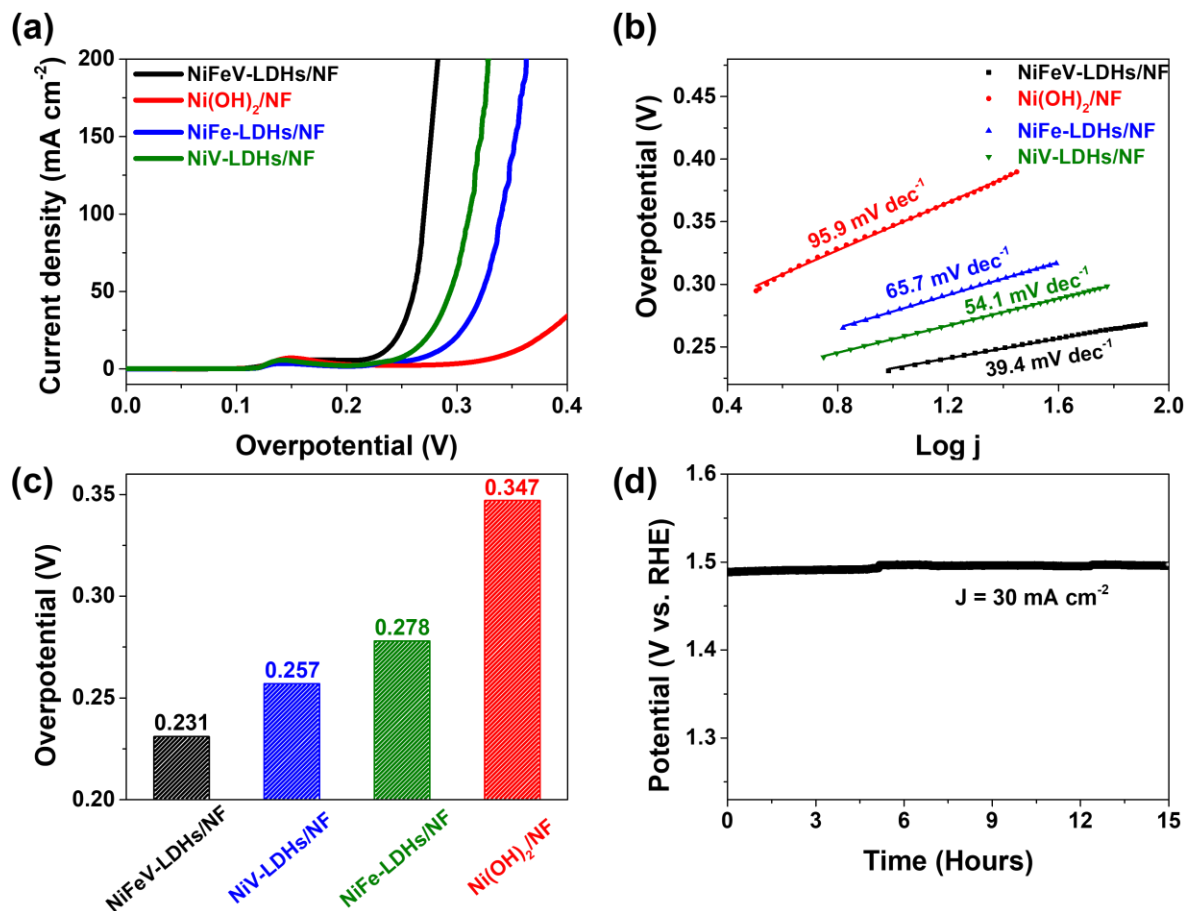
## Figures and Captions.

Figure 1. Khang Ngoc Dinh *et al.*

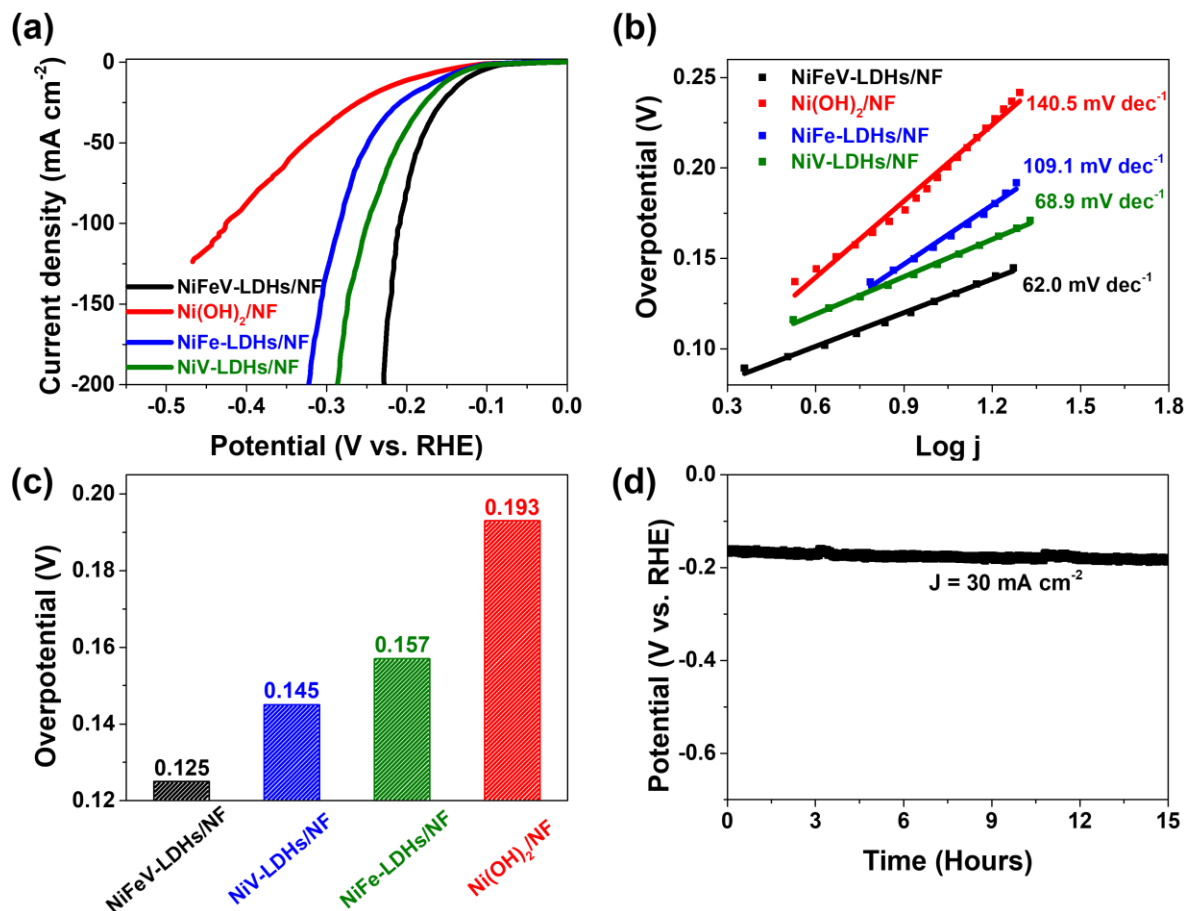
**Figure 1.** (a) XRD spectra of NiFeV-LDHs/NF (in red) and Ni(OH)<sub>2</sub>/NF (in black, synthesized without the Fe and V precursor). (b-d) XPS spectra of NiFeV-LDHs/NF in (b) Ni 2p region, (c) Fe 2p region, and (d) V 2p region.

Figure 2. Khang Ngoc Dinh *et al.*

**Figure 2.** (a) FESEM image, (b,c) TEM images, (d) HRTEM image, (e) SAED pattern. (f) HAADF-STEM image and (h-j) its corresponding STEM-EDX elemental mappings of (g) Ni, (h) Fe, and (i) V of NiFeV-LDHs nanosheets.

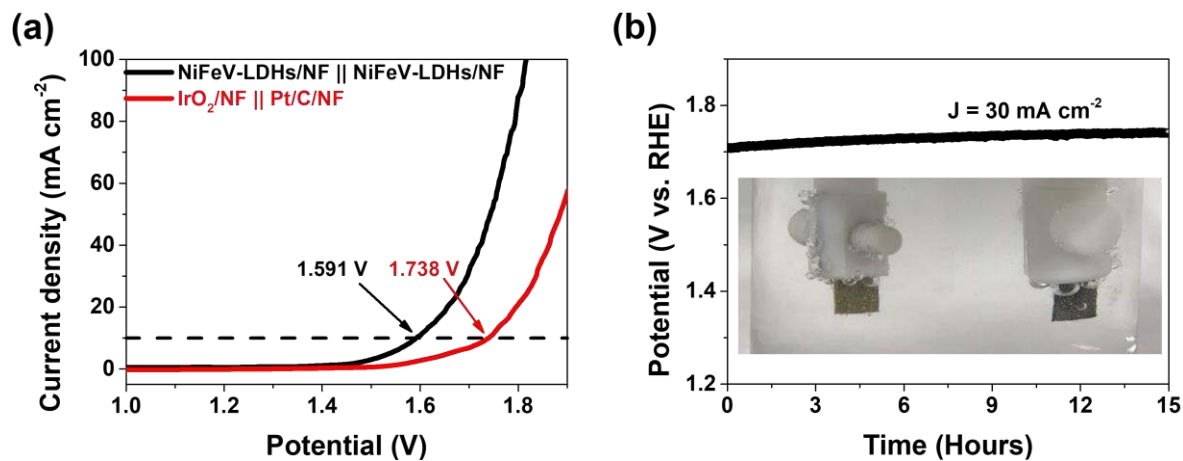
Figure 3. Khang Ngoc Dinh *et al.*

**Figure 3.** (a) OER polarization curves of NiFeV-LDHs/NF, Ni(OH)<sub>2</sub>/NF, NiFe-LDHs/NF, and NiV-LDHs/NF in 1.0 M KOH at scan rate of 1.0  $\text{mV s}^{-1}$  and their corresponding (b) Tafel slopes. (c) The overpotentials of above samples at the current density of 10  $\text{mA cm}^{-2}$ . (d) Chronopotentiometry measurements of NiFeV-LDHs/NF electrode at the current density of 30  $\text{mA cm}^{-2}$  in 1.0 M KOH solution.

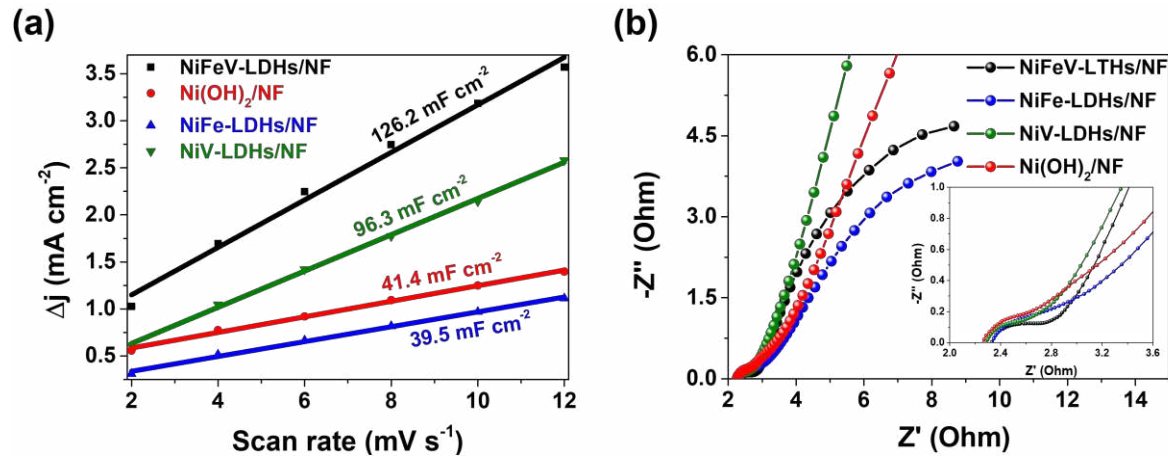
Figure 4. Khang Ngoc Dinh *et al.*

**Figure 4.** (a) HER polarization curves of NiFeV-LDHs/NF, Ni(OH)<sub>2</sub>/NF, NiFe-LDHs/NF, and NiV-LDHs/NF in 1.0 M KOH at scan rate of 1.0  $\text{mV s}^{-1}$  and their corresponding (b) Tafel slopes. (c) The overpotentials of above samples at the current density of 10  $\text{mA cm}^{-2}$ . (d) Chronopotentiometry measurements of NiFeV-LDHs/NF electrode at the current density of 30  $\text{mA cm}^{-2}$  in 1.0 M KOH solution.



Figure 5. Khang Ngoc Dinh *et al.*

**Figure 5.** (a) Polarization curves of the water electrolysis using NiFeV-LDHs/NF as bifunctional electrocatalyst compared with IrO<sub>2</sub>/NF || Pt/C/NF in a two-electrode system at the scan rate of 1.0 mV s<sup>-1</sup> (b) Chronoamperometric response (inset: image taken during water splitting).

Figure 6. Khang Ngoc Dinh *et al.*

**Figure 6.** (a) Plot of capacitive currents density ( $j_{\text{anodic}}-j_{\text{cathodic}}$ ) at 0.35 V vs. Hg/HgO as a function of various scan rates and (b) EIS spectrum measured at 300 mV overpotential of Ni<sub>0.75</sub>Fe<sub>0.125</sub>V<sub>0.125</sub>-LDHs/NF, Ni<sub>0.75</sub>Fe<sub>0.25</sub>-LDHs/NF, Ni<sub>0.75</sub>V<sub>0.25</sub>-LDHs/NF, Ni(OH)<sub>2</sub>/NF.

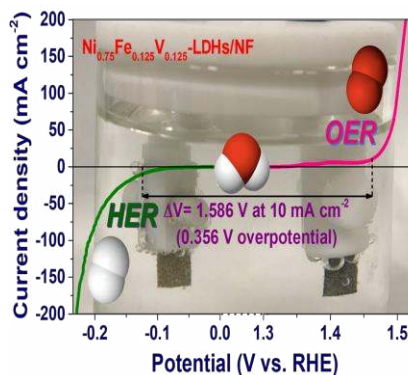
Porous ultrathin  $\text{Ni}_{0.75}\text{Fe}_{0.125}\text{V}_{0.125}$  layer double hydroxide (LDHs) nanosheets grown on Ni foam (NF) is successfully prepared. The  $\text{Ni}_{0.75}\text{Fe}_{0.125}\text{V}_{0.125}$ -LDHs/NF electrode shows exceptional performances toward OER and especially HER in alkaline solution. Interestingly, only a single battery unit of 1.5 V can drive the water electrolysis, outperforming the state-of-the-art  $\text{IrO}_2/\text{NF}||\text{Pt}/\text{C}/\text{NF}$  and indicating successful overall water splitting with barely 0.27 V overpotential.

**Keyword:** Overall water splitting; two-dimensional materials; layer double hydroxides; electrocatalysis; porous nanosheets

K. N. Dinh, P. L. Zheng, Z. F. Dai,\* Y. Zhang, R. Dangol, Y. Zheng, B. Li, Y. Zong, and Q. Yan\*

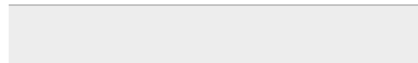
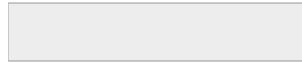
### Ultrathin Porous NiFeV Ternary Layer Hydroxide Nanosheets as a Highly Efficient Bifunctional Electrocatalyst for Overall Water Splitting

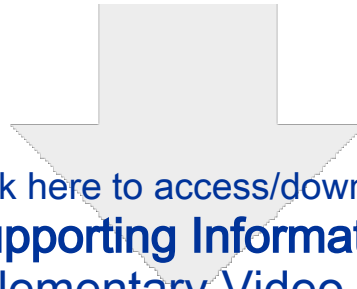
ToC figure



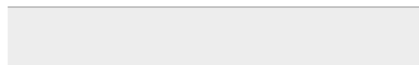
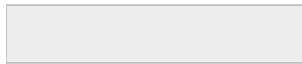


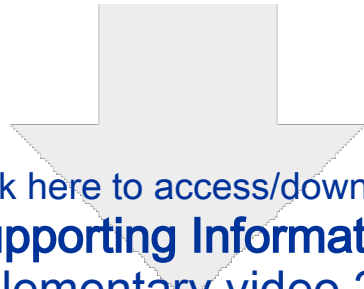
Click here to access/download  
**Supporting Information**  
Supporting Information revised.doc



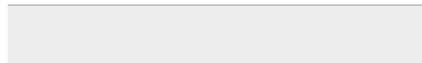
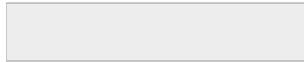


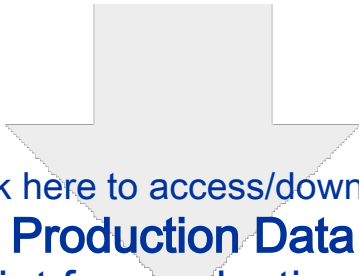
Click here to access/download  
**Supporting Information**  
Supplementary Video 1.mp4



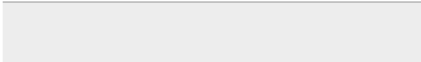
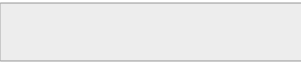



Click here to access/download  
**Supporting Information**  
Supplementary video 2.mp4





Click here to access/download  
**Production Data**  
Manuscript for production data.doc

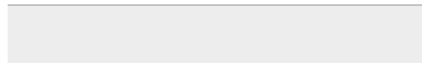
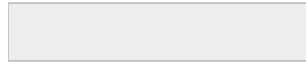




[Click here to access/download](#)

**Production Data**

Supplementary Video 1 for production data.mp4



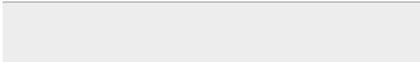
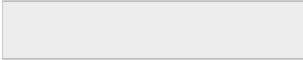




[Click here to access/download](#)

**Production Data**

[Supplementary Video 2 for production data.mp4](#)

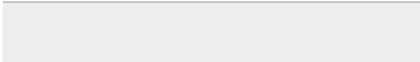
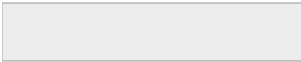




Click here to access/download

**Production Data**

Supporting Information for production data.doc





[Click here to access/download](#)

**Production Data**

[Table of Contents for production data.doc](#)

